



## Article

# A New Line Matching Approach for High-Resolution Line Array Remote Sensing Images

Jingxue Wang <sup>1,\*</sup>, Suyan Liu <sup>1</sup> and Ping Zhang <sup>2</sup><sup>1</sup> School of Geomatics, Liaoning Technical University, Fuxin 123000, China; 471720212@stu.lntu.edu.cn<sup>2</sup> College of Environmental Art and Architectural Engineering, Heilongjiang University of Technology, Jixi 158100, China; 471820535@stu.lntu.edu.cn

\* Correspondence: wangjingxue@lntu.edu.cn

**Abstract:** In this paper, a new line matching approach for high-resolution line array remote sensing images is presented. This approach establishes the correspondence of straight lines on two images by combining multiple constraints. Firstly, three geometric constraints, epipolar, direction and the point-line geometric relationship, are used in turn to reduce the number of matching candidates. After this, two similarity constraints, the double line descriptor and point-line distance, are used to determine the optimal matches. Finally, the co-linearity constraint is used to check the one-to-many and many-to-one correspondences in the results. The proposed approach is tested on eight representative image patches selected from the ZY-3 line array satellite images, and the results are compared with those of two state-of-the-art approaches. Experiments demonstrate the superiority and potential of the proposed approach due to its higher accuracy and greater number of matches in most cases.

**Keywords:** high-resolution line array remote sensing images; line matching; line descriptor; epipolar constraint; corresponding points constraint



**Citation:** Wang, J.; Liu, S.; Zhang, P. A New Line Matching Approach for High-Resolution Line Array Remote Sensing Images. *Remote Sens.* **2022**, *14*, 3287. <https://doi.org/10.3390/rs14143287>

Academic Editors: Wanshou Jiang, Xiongwu Xiao and San Jiang

Received: 19 May 2022

Accepted: 4 July 2022

Published: 8 July 2022

**Publisher's Note:** MDPI stays neutral with regard to jurisdictional claims in published maps and institutional affiliations.



**Copyright:** © 2022 by the authors. Licensee MDPI, Basel, Switzerland. This article is an open access article distributed under the terms and conditions of the Creative Commons Attribution (CC BY) license (<https://creativecommons.org/licenses/by/4.0/>).

## 1. Introduction

The availability of high-resolution optical satellite remote sensing images has increased significantly with the rapid development of space technology. Image matching is one of the most significant phases of image-based 3D reconstruction. The existing feature point-based quasi-dense matching or pixel-based dense matching can successfully obtain the general contour of the object, but the edges of artificial ground object models such as buildings can experience problems such as boundary deformation. Compared to feature point, the feature line in an image can more accurately express the contour features of the object. Therefore, line matching plays a key role in computer vision [1], image registration [2] and 3D reconstruction [3–5]. Line matching serves to establish correspondence between corresponding lines from different images using image correlation techniques. The existing line matching approaches can be divided into three categories, described below.

The first is line matching based on geometric properties. The main geometric properties commonly used are length, overlapping, distance, gradient, etc. [6–9]. Due to the uncertainty of the endpoints of lines and lines that are broken during line segment extraction, a line matching algorithm with a single geometric constraint matching is insufficient. Therefore, a combination of multiple constraints is mostly used in the line matching process. Here, the existing geometric constraints, such as epipolar constraint [10,11], triangulation constraint [12] and line-point invariant constraint [13,14], are often used. Among them, the most preferred constraint is probably the epipolar constraint, which can limit the matching candidates to a small quadrilateral region and is often used as a benchmark for determining the corresponding direction of two images. Zhang et al. [15] used the corresponding Delaunay triangulations, constructed by reliable corresponding points, to constrain the

initial matching candidates, and the final line-to-line correspondence was determined by a gray correlation method based on adaptive moving windows. Fan et al. [16] proposes a matching approach that is mainly based on the affine invariance of the line and points that are located around the line segment, which are assumed to be coplanar located with the line in 3D space.

The second type of approach is line matching based on a line descriptor. A line descriptor is constructed to describe the local features of the line, and line matching is achieved by measuring the similarity between the line descriptors [17–19]. Schmid et al. [20] achieved line matching by comparing the gray correlation of line neighborhood windows. Bay et al. [21] constructed a color histogram as a local line descriptor and used a topological filter to remove incorrect candidates. A similarity measure based directly on gray information is affected by light variation and the robustness of the descriptors is low. Along with SIFT generation [22], gradient-based descriptors are becoming increasingly popular. Wang et al. [23] proposed a SIFT-like descriptor called the mean–standard deviation line descriptor (MSLD). It first defines the parallel neighborhood of the line as the pixel support region, which is then partitioned to be used for the gradient statistics, and the mean and standard deviation of the gradient statistics for the different partitions are calculated to generate the line descriptor. To overcome the fact that MSLD descriptors are not scale-invariant, Verhagen et al. [24] proposed a scale-invariant mean–standard deviation line descriptor (SMSLD) for wide baseline matching. Inspired by Ref MSLD, Zhang et al. [25] proposed the LBD descriptor. Unlike MSLD, which divides the support region vertically, LBD divides the support region in a parallel line direction. Each sub-region is referred to as a band. Gradient statistics are performed for each band, considering both its upper and lower bands, while the global Gaussian weight function and the local Gaussian weight function are applied to each row of the region of interest.

The third type of approach is line matching based on the line pair feature. These methods take as matching primitives the line pairs that are generated by grouping two lines that satisfy certain geometric relationships. Ideally, the two lines in the pair satisfy coplanarity in object space. The similarity of geometric features between both line segments during the matching process is fully employed to establish pair-to-pair correspondence. The geometric properties that are often used include the distance between both line segments, the intersection angle between both lines, the ratio of the lengths of two line segments, the intersection point between both lines and the descriptor of the neighborhood that is centered on the intersection point [26–30]. To increase the probability that two lines in the pair are coplanar, Li et al. [31] has constructed a neighborhood window of the line during the grouping process, where two lines whose endpoints and intersections are within the window are considered as coplanar lines and paired. Based on the epipolar constraint, Alshahri et al. [32] used the corresponding points in the neighborhood of two hypothetical matching pairs to calculate the local homography matrix, which was used to constrain the subsequent matching. In the process of line pair matching, Wang et al. [33] and Park et al. [34] used the endpoints, midpoints and intersection point of two lines in a line pair to construct line geometric topological relationships, and further established similarity constraints for matching lines. In addition to geometric information, Ok et al. [35] added the radiometric information of the line pair neighborhood. Referring to the point-based Daisy gradient descriptor, a line-based Daisy gradient description was constructed for the similarity measure. A combined similarity measure was defined by assigning different weights to each metric, and the NNDR criterion was applied to check the matching results and find the optimal line-to-line matches by iteration.

Compared to individual line matching, line pair matching is more time-consuming and complex due to the additional work that is involved in the pairing and post-processing of line-to-line correspondences. Therefore, individual line matching is more suitable for the broad coverage of line array satellite remote sensing images. In our approach, two strong geometric constraints, the epipolar and the corresponding points, are used to narrow down the matching candidates, which effectively improves the reliability of matching candidates

and enhances the matching efficiency. During descriptor construction, the determination of corresponding support regions and the construction of descriptors on each side of the line segment are considered simultaneously. The construction of double descriptors resolves false matches that are caused by inconsistencies in the corresponding support regions of the corresponding lines on both images.

The remainder of this paper is organized as follows. Section 2 introduces our new line matching approach for high-resolution line array remote sensing images and details the geometric constraints and similarity constraints in the line matching process. Section 3 describes the test datasets that are used for line matching, the parameter selection for key parameters and the comparative analysis of different methods. Finally, Section 4 summarizes the methods that are used in this study and presents opportunities for future studies.

## 2. Methodology

Line matching can be seen as a search process. We take a set of stereo images as an example. One image is selected as the reference image, and the other one acts as the search image. Assume that the number of lines that are extracted from the reference image and the search image are  $a$  and  $b$ , respectively. A line,  $l_i$ , on the reference image is selected to be matched, called the target line or reference line, and all lines or some lines that satisfy the constraints on the search image are considered as candidate lines. The similarity measure  $\rho$  between the target line and each of the candidate lines on the search image is calculated separately, where the candidate line corresponding to the maximum similarity measure is the corresponding line of the target line, i.e., when  $\rho(l_i, l'_k) = \max\{\rho(l_i, l'_j), j = 1, 2, 3, \dots, c; c \leq b\}$ ; ( $i = 1, 2, 3, \dots, a$ ), then  $(l_i, l'_k)$  is considered to be a pair of corresponding lines.  $\rho(l_i, l'_j)$  indicates the similarity measure between the line  $l_i$  on the reference image and the line  $l'_j$  on the search image.

This paper presents a new line matching approach for high-resolution line array remote sensing images, and the overall methodology is shown in Figure 1. The input data for our approach consists of two remote sensing images and their rational polynomial coefficient (RPC). One image is selected as the reference image and the other one acts as the search image. We start with the extraction of the feature line segments and the acquisition of initial reliable corresponding points from both images. The former uses the LSD algorithm [36] for feature line extraction, while the latter first uses the SIFT algorithm [22] to obtain the corresponding points, and then applies the RANSAC algorithm [37] to check the matching results to remove false matches. In the initial matching phase, we use the epipolar constraint to select the initial matching candidates, followed by the direction constraint and the corresponding points constraint, which are used in turn to reduce the number of candidates. In the second matching phase, the line descriptor similarity and points–line distance are used to determine the optimal matching results. In the post-processing phase, the co-linearity constraint is used to check the one-to-many and many-to-one results for the final line correspondences.

### 2.1. Epipolar Constraint

#### 2.1.1. Epipolar Line Generation

The epipolar constraint is one of the most popular geometric constraints that is used in image matching. It has the effect of reducing the search range and improving the matching efficiency. For high-resolution line array satellite remote sensing images, this paper iteratively constructs its inverse solution model with the positive solution parameters of the rational function model (RFM) of the line array image. Corresponding epipolar lines are generated by combining the RFM inverse solution model with the projected trajectory method [38]. Figure 2a,b represent the reference image and search image, respectively, and the blue lines are the corresponding epipolar lines on both images.

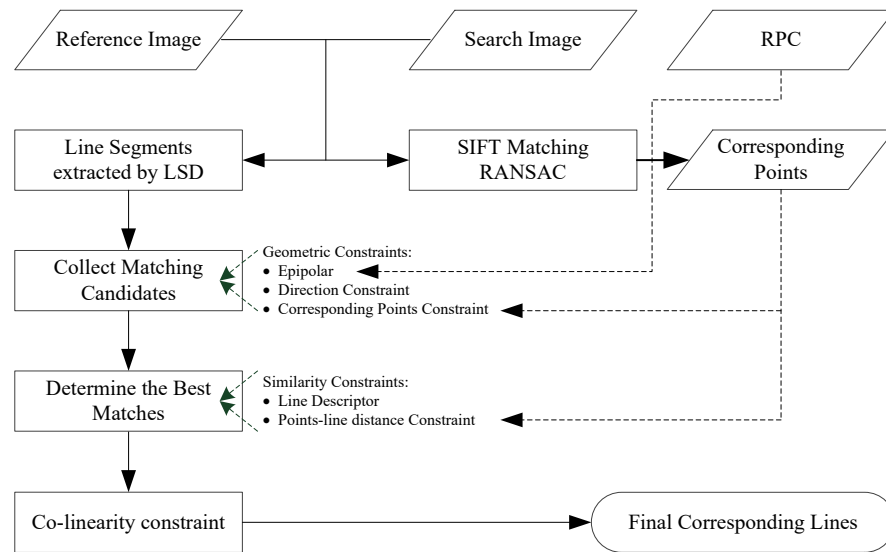


**Figure 1.** Flowchart of proposed line matching approach.

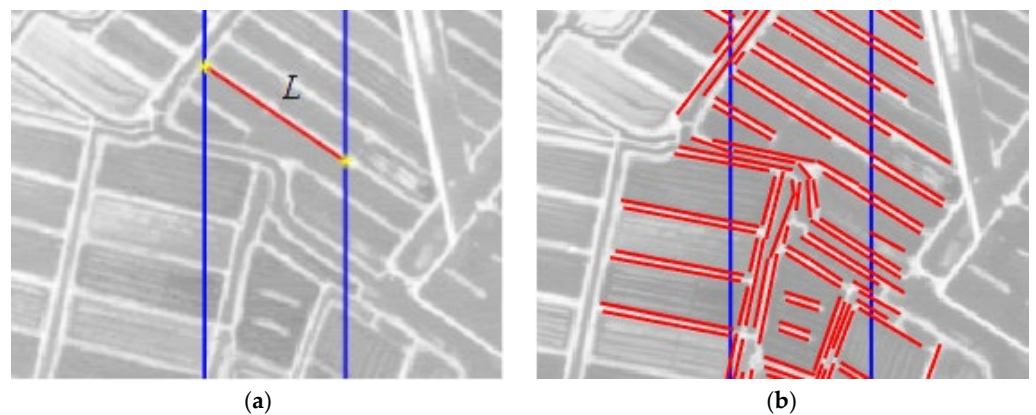


**Figure 2.** Overlap constraint. (a) Reference image; (b) search image.  $L$  is the reference line on the reference image and the blue lines on both images are the corresponding epipolar lines for the endpoints of the  $L$ . The red feature lines on the search image are a set of candidates that satisfy the overlap constraint.

### 2.1.2. Overlap Constraint

Due to the influence of the radiometric variation on different images and the line extraction algorithm, there are some differences in the extraction results of the corresponding feature line on different images, such as non-corresponding line segment endpoints and different segment fragmentation. Based on the condition that there should be an overlapping segment between corresponding lines in different views, we determine matching candidate line segments using the epipolar constraint. The process is implemented as follows, calculating the epipolar lines of the two endpoints of the reference line segment using the above-mentioned epipolar generation method. The line segment on the search image that intersects at least one of the two epipolar lines or is within the range of the two epipolar lines is considered as a candidate line. Inspired by Ref [32], the Boolean operator formula to satisfy this constraint is shown in Formula (1):

$$C_{l,l'} = \begin{cases} ((c'_x - d_x)(c_x - c'_x) > 0) \vee \\ ((d_x - d'_x)(c'_x - d_x) > 0) \vee \\ ((d'_x - d_x)(c_x - d'_x) > 0) \vee \\ ((c_x - d'_x)(c'_x - c_x) > 0) \end{cases} \quad (1)$$

where  $\vee$  represents the logical “or” relationship.  $C_{l,l'}$  denotes a pair of correspondence hypotheses  $(l, l')$ , where  $l$  and  $l'$  represent the reference line and candidate line, respectively.  $c$  and  $d$  represent the two endpoints of the candidate line segment, and  $c'$  and  $d'$  represent the intersection points of the candidate line segment and both epipolar lines on the search image, in which the subscript  $x$  denotes the  $x$ -coordinates. If the  $C_{l,l'}$  is true, then the correspondence hypothesis  $(l, l')$  satisfies the overlap constraint. Figure 2 presents an example of the overlap constraint.

## 2.2. Direction Constraint

During the matching of line segments, the epipolar constraint is a two-dimensional constraint, and the number of candidates in the epipolar quadrilateral region could be excessive. Therefore, other strong geometric constraints can be employed to reduce the candidates, and the direction constraint is one of them. We take the corresponding epipolar lines on the two images as the reference and calculate the angles between the lines to be matched on the two images and the corresponding epipolar lines separately. At first, corresponding epipolar lines passing through the midpoint of the reference line are generated. Then, the angle of the reference line to the epipolar line on the reference image and the angle of the candidate line to the epipolar line on the search image are calculated, respectively, and denoted as  $\theta_r$  and  $\theta_c$ . The difference between the above two angles is calculated and compared with a given threshold value,  $T_\theta$ . If the absolute value of the difference is less than the given threshold, i.e.,  $|\theta_r - \theta_c| < T_\theta$ , then the candidate line satisfies the direction constraint; otherwise, it is discarded. Based on the results of the epipolar constraint in Figure 2, the direction constraint results are obtained, as shown in Figure 3.

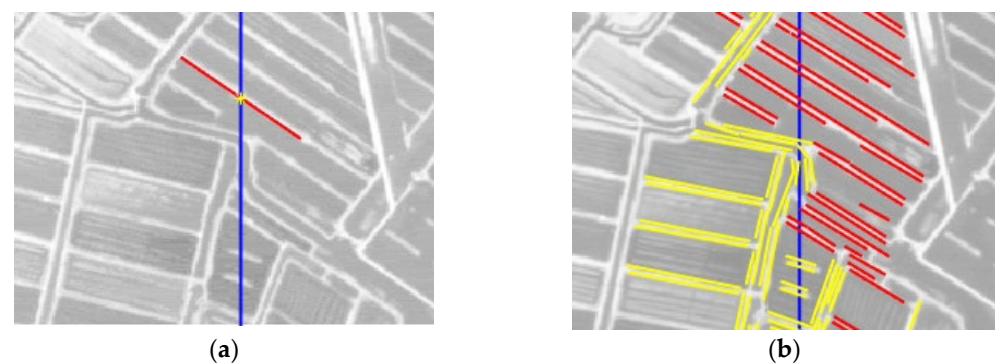


**Figure 3.** Direction constraint. (a) Reference image; (b) search image. The blue lines on both images are the corresponding epipolar lines for the midpoint of the  $L$ . The red lines in (b) are the candidate lines to be retained as satisfying the direction constraint, and the yellow lines are those filtered out by the direction constraint.

## 2.3. Corresponding Points Constraint

After the above two constraints, the matching candidates are limited in a relatively small range, but for the repeated texture region, due to the existence of parallel feature lines, there is still a relatively large number of matching candidates after applying the direction constraint. Therefore, based on the consistency of the local geometric relationships between corresponding points and corresponding lines on different views, we further narrow down the candidates with the matched points, i.e., the local geometric relationship between a line and its neighboring matched points is used. We first determine the matched points in the neighborhood of the reference line. Suppose that a reference line  $L$  with length  $l$  makes a line  $L_\perp$ , which passes through the midpoint of the line  $L$  and is perpendicular to the line  $L$ . The matched points that satisfy the condition wherein the distance to the line  $L$  is less than  $T_{D1}$  and the distance to the line  $L_\perp$  is less than  $T_{D2}$  are selected as the points in the neighborhood of the line  $L$ . In other words,  $d(p_i, L) < T_{D1}$  and  $d(p_i, L_\perp) < T_{D2}$ , where  $d(\cdot)$  denotes the distance from the point to the line,  $p_i$  is a matched point.  $T_{D1}$  and  $T_{D2}$  are the

distance thresholds, such that  $T_{D2} = l/2 + \Delta$ , where  $\Delta$  is expressed as the distance from each end of the line segment  $L$  extended outward. In this paper,  $\Delta = 30$ . The set of matched points in the neighborhood of the line  $L$  is recorded as  $S$ , which corresponds to the set of points on the search image as  $S'$ . At the same time, the points on both sides of the line segment  $L$  are denoted as set  $P_+$  and set  $P_-$ , respectively, and  $S = P_+ \cup P_-$ . Take a candidate line to be checked on the search image as the reference, and the points in the set  $S'$  that are located on both sides of the candidate line are recorded as sets  $P'_+$  and  $P'_-$ , respectively. If the above four sets satisfy the condition  $(P_+ = P'_+ \& P_- = P'_-) \vee (P_+ = P'_- \& P_- = P'_+)$ , the candidate line is retained; otherwise, it is removed. Here,  $\vee$  represents the logical “or” relationship and  $\&$  represents the logical “and” relationship. Based on the results of the direction constraint in Figure 3, the corresponding constraint results are shown in Figure 4b. As shown in Figure 4, for candidates on the search image that satisfy the conditions, the matched points in blue are located under the candidate line, and the matched points in red are located above the candidate line, which is consistent with the local geometric relationship between the matched points and the reference line on the reference image.

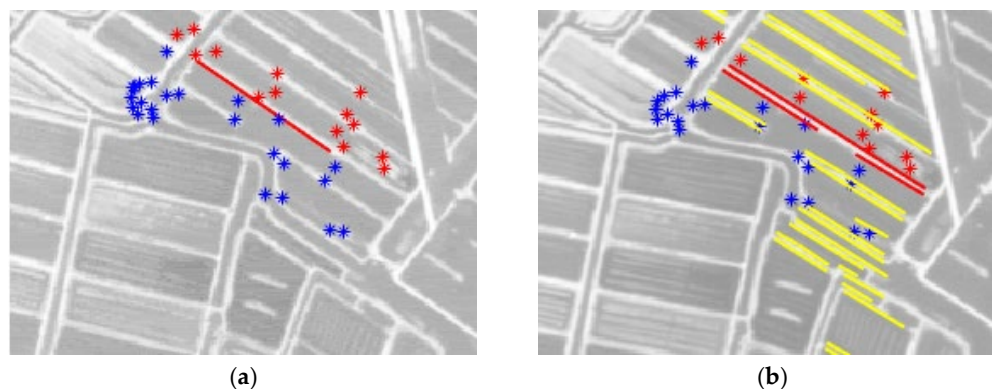


**Figure 4.** Corresponding points constraint. (a) Reference image; (b) search image. The blue points and the red points are the corresponding points on both images, respectively, on either side of the reference line. The red lines in (b) are the candidate lines to be retained as satisfying the corresponding points constraint, and the yellow lines are those filtered out by the corresponding points constraint.

## 2.4. Similarity Constraint for Line Descriptor

### 2.4.1. Generation of the Line Support Region

For each candidate line that satisfies the above constraints, it is further judged whether it satisfies the descriptor similarity constraint. Based on the principle of the line band descriptor (LBD) that is proposed by Zhang [25], the affine transformation of the support region is added, while the LBD descriptors on both sides of the line are generated separately. To construct the corresponding support regions of the corresponding lines, the epipolar lines of the endpoints of the two lines in the candidate matching pair are used to determine the corresponding maximum overlap segments between two lines. As shown in Figure 5b, the two candidate lines are each extended to the epipolar lines.

On the reference image, a rectangular region centered at the line  $L$  is generated as the line support region, as shown in Figure 6. The size of the support region is  $c \times len$ , where  $len$  is the length of the rectangle, which is equal to the length of the line  $L$ , and  $c$  is the width of the rectangle. To make the descriptor rotation-invariant and facilitate the following calculations, the support region is affine transformed so that it is parallel to the image coordinate system, and the size of the region remains the same before and after the affine transformation. The support region is divided into  $m$  bands  $\{B_1, B_2 \dots B_m\}$ , where each band is a sub-region and parallel to the horizontal direction, and the width of a band is  $w$ . Thus,  $w \times m = c$ . In the diagram, assume  $m = 5$ .

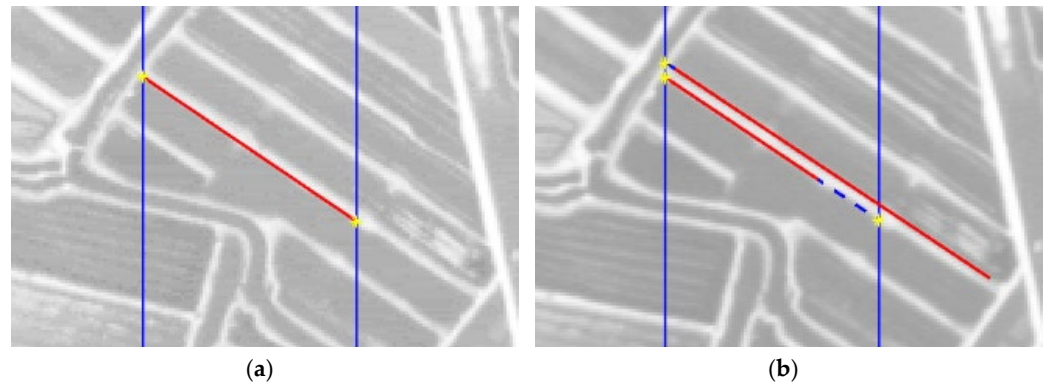


**Figure 5.** Determining the corresponding segments. (a) Reference image; (b) search image. The blue lines on both images are the corresponding epipolar lines for the endpoints of the  $L$ . The line segment with the intersections of the candidate line and the two epipolar lines as endpoints is the overlapping segment of the candidate line corresponding to the reference line.

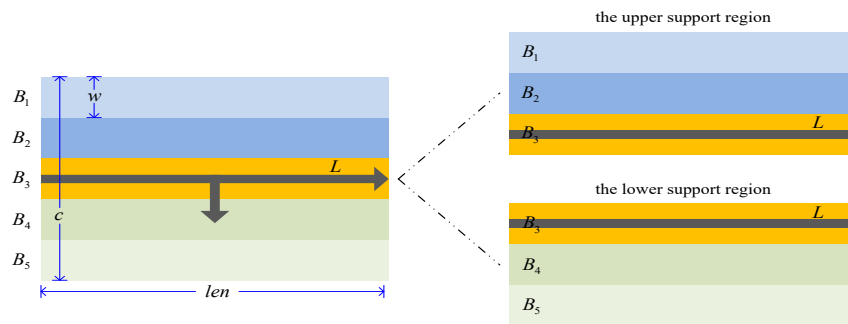


**Figure 6.** Construction of the line support region. The support region of line  $L$  has size  $c \times len$ , and is divided into 5 bands, each of width  $w$ . The upper and lower support regions contain the first three bands and the last three bands, respectively, for the construction of descriptors on each side of the line.

### 2.4.2. The Construction of the Line Descriptor

The gradient descriptor of a line, known as the line descriptor, is a gradient orientation statistic for pixels within the line neighborhood in sub-regions. Each statistic value is the sum of the gradient magnitudes near that direction within the sub-region. A different weight is given to each pixel during the statistics based on the distance from the pixel to the line. A line descriptor is a vector containing the gradient statistics of all the different sub-regions, or a vector consisting of the mean vector or vector normalization of the statistics of the corresponding orientations within all the different sub-regions.

To enhance the robustness of the line descriptor, we divide the support region into two parts, which are used to construct the line descriptor separately. Assume that the band in which the line segment is located is the  $i$ -th band, denoted as  $B_i$ . Then, the region from band  $B_1$  to band  $B_i$  is one part, and the region from band  $B_i$  to band  $B_m$  is another part, denoted as the upper and lower support regions of the line segment, respectively. Correspondingly, the line descriptors that are constructed from the above two regions are denoted as  $LBD_u$  and  $LBD_l$ , respectively.

$$\begin{aligned} LBD_u &= (BD_1^T, BD_2^T, \dots, BD_i^T)^T \\ LBD_l &= (BD_i^T, BD_{i+1}^T, \dots, BD_m^T)^T \end{aligned} \tag{2}$$

where  $BD_k$  is the band descriptor of the  $k$ -th band, which is computed from band  $B_k$  and its nearest two neighbor bands  $B_{k-1}, B_{k+1}$ . Specifically, any band that is outside of the support region will not be considered when calculating the band descriptor for the top and bottom bands  $B_1, B_i$  and  $B_m$ . Now, we construct the band descriptor  $BD_k$ . For the row  $B_k^h$ , the  $h$ -th

row in band  $B_k$  and its neighboring bands, we accumulate the gradients of pixels within this row along four directions ( $0^\circ, 90^\circ, 180^\circ, 270^\circ$ ), respectively,

$$V_k^h = ((V_k^h)_1, (V_k^h)_2, (V_k^h)_3, (V_k^h)_4)^T \in \mathbb{R}^{4 \times 1} \quad (3)$$

$$\begin{cases} (V_k^h)_1 = \lambda_k^h \cdot \sum_{\text{pixel} \approx 0^\circ} g_{\text{pixel}} & , \quad (V_k^h)_2 = \lambda_k^h \cdot \sum_{\text{pixel} \approx 90^\circ} g_{\text{pixel}} \\ (V_k^h)_3 = \lambda_k^h \cdot \sum_{\text{pixel} \approx 180^\circ} g_{\text{pixel}} & , \quad (V_k^h)_4 = \lambda_k^h \cdot \sum_{\text{pixel} \approx 270^\circ} g_{\text{pixel}} \end{cases} \quad (4)$$

In Formula (4),  $\lambda_k^h$  is the weight coefficient of the row  $B_k^h$ , which is related to two Gaussian weighting functions that are applied to each row of the line support region along the column direction. One is a global weighting coefficient  $f_g(i) = (1/(\beta\sqrt{\pi}))e^{-(d_i/\beta)^2}$ , where  $\beta = \sqrt{\Gamma(1/2)/\Gamma(3/2)}$ ,  $i$  denotes the  $i$ -th row of the line support region, and  $d_i$  is the distance of the  $i$ -th row to the row where the line segment is located. The other is a local weighting coefficient  $f_l(B_k^h) = (1/\beta\sqrt{\pi})e^{-(d_h/\beta)^2}$ , in which  $d_h$  is the distance of the row  $B_k^h$  to the center row of  $B_k$ . Thus,  $\lambda_k^h = f_g(j)f_l(B_k^h)$ , where it is assumed that the row  $B_k^h$  is the  $j$ -th row of the line support region.

By stacking these four accumulated gradients of all the rows that are associated with band  $B_k$ , the band gradient description matrix (GDM) is formed as follows:

$$GDM_k = (V_k^1, V_k^2, \dots, V_k^n) \in \mathbb{R}^{4 \times n} \quad (5)$$

where  $n$  is the number of rows that are associated with  $B_k$ . The mean vector  $M_k$  of  $GDM_k$  row vectors is computed to obtain the descriptor of band  $B_k$ , and  $BD_k = (M_k) \in \mathbb{R}^{4 \times 1}$ . Through substitution in Equation (2), the descriptors  $LBD_u$  and  $LBD_l$  of both support regions of the line segment are obtained, respectively,

$$\begin{aligned} LBD_u &= (M_1^T, M_2^T, \dots, M_i^T) \in \mathbb{R}^{4i \times 1} \\ LBD_l &= (M_i^T, M_{i+1}^T, \dots, M_m^T) \in \mathbb{R}^{4i \times 1} \end{aligned} \quad (6)$$

### 2.4.3. Similarity Constraint

Similarly, for a candidate line on the search image, the line support region is constructed with the overlapping segment corresponding to the reference line as the center, and the candidate line descriptors  $LBD'_u$  and  $LBD'_l$  are obtained. The Euclidean distance formula is used to calculate the similarity of the two descriptors. For a reference line and a candidate line, two similarities are computed, corresponding to the descriptors of the upper and lower support regions of the two lines, respectively. As long as one of the two similarities is less than a given threshold,  $T_d$ , the candidate line is considered to satisfy the similarity constraint.

### 2.5. Determining the Final Matching Results

After applying the four constraints that are described above, there may still be many candidates for the reference line. We combine the point–line distance constraint and the collinearity constraint to determine the final matching results. According to Section 2.3, we have obtained two sets of matching points,  $P_+$  and  $P_-$ , which are located on either side of the reference line, and the corresponding sets of matching points,  $P'_+$  and  $P'_-$ , which are located on either side of the candidate line on the search image. We calculate the sum of the distances from all points in each set to the line, respectively, according to Formula (7),

$$\begin{aligned} D_+ &= \sum_{p_j \in P_+} d(p_j, l_r), D_- = \sum_{p_k \in P_-} d(p_k, l_r) \\ D'_+ &= \sum_{p'_j \in P'_+} d(p'_j, l_c), D'_- = \sum_{p'_k \in P'_-} d(p'_k, l_c) \end{aligned} \quad (7)$$

where  $p_j, p_k, p'_j$  and  $p'_k$  denote any point in the set.  $l_r$  and  $l_c$  denote the reference line and the candidate line, respectively. If the condition  $(abs(D_+ - D'_+) < T_{D3}) \vee (abs(D_- - D'_-) < T_{D3})$  is satisfied, it means that the candidate line satisfies the point–line distance constraint, where  $T_{D3}$  is the threshold. For any reference line, if only one candidate satisfies the condition, then the candidate line is the final corresponding line. If there are still many candidates satisfying the constraint, we first judge whether these candidate lines are co-linear. If they are, then all the candidates are correct matches; otherwise, the line corresponding to the smallest distance difference among the candidates is selected as the correct match.

When all the lines have been matched, we check whether there are “many-to-one” matching correspondences between two images in the results, i.e., many lines on the reference image correspond to the same line on the search image. If so, we identify the final match in the same way as above with the collinearity constraint and the point–line distance constraint.

### 3. Line Matching Experiments

To evaluate the performance of our approach, we selected eight pairs of image patches from the forward- and backward-looking image pairs of the ZY-3 satellite for line matching experiments, as shown in Figure 7. The ground sampling distance of the image is approximately 3.5 m. These image patches were chosen to represent the characteristics of different landscapes, including farmland, paddy fields, residential environments with dense and complex buildings, countryside, etc. Among them, the smallest image size is 400 pixels  $\times$  400 pixels, as shown in Figure 7c, and the largest image size is 600 pixels  $\times$  600 pixels, as shown in Figure 7b. In this study, the experiments were performed on a 1.60 GHz Intel (R) Core(TM) i5-4200U CPU processor with 8 GB of RAM.

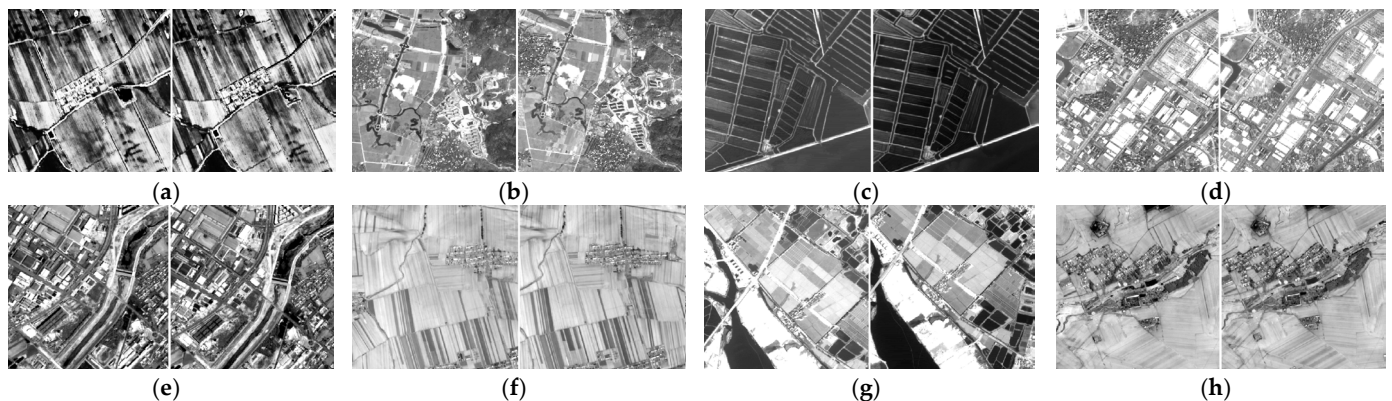


**Figure 7.** The image patches selected from the ZY-3 satellite images. Farmland (a,f); countryside (b,h); paddy fields (c,g); buildings (d,e).

#### 3.1. Parameter Selection

Several parameters are adopted in our approach, four of which are key and influence the performance of the approach. To balance the impact of these parameters on matching, two image pairs, Figure 7a,b, were randomly selected for parameter analysis experiments to determine their thresholds. Each parameter’s value was determined by a comparative analysis of the matching results under different parameter values.

##### 3.1.1. Determine the Value of Parameter $T_\theta$

$T_\theta$  is the threshold value for the direction constraint. This is reflected in the matching by the fact that the angles between two lines in a candidate pair and their corresponding epipolars should be approximately equal. Due to errors such as linear extraction and epipolar computation, there will be a small deviation between two angles. Therefore, given other parameter values, the two sets of images in Figure 7a,b are matched with values of  $T_\theta$  at 5°, 10°, 15°, 20° and 25°, respectively, and the results are shown in Figure 8. For both

image pairs, both the number of matches and the number of correct matches in the results peak in the rate of change at  $T_\theta = 10^\circ$  and stabilize at  $T_\theta = 15^\circ$ . Image pair (b) reaches the peak of matching accuracy at  $T_\theta = 10^\circ$ , and the matching accuracy of image pair (a) shows a decreasing trend as the threshold value increases. Thus,  $T_\theta = 10^\circ$  is selected in this paper.

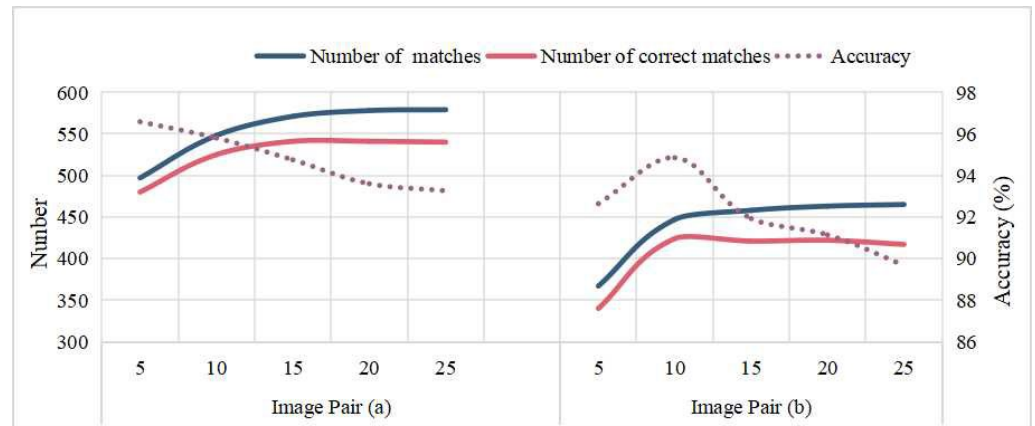


Figure 8. Performance of our approach with different  $T_\theta$  for Figure 7a,b image pairs.

### 3.1.2. Determine the Values of Parameters $m$ and $w$

$m$  and  $w$  are two parameters that are involved in the construction of the support region for the descriptor.  $m$  is the number of bands in the support region and  $w$  is the width of each band. These two parameters together determine the size of the support region. Under the conditions that  $w$  takes the values of 3, 5, 7, 9 and 11, respectively, and  $m$  takes the values of 3, 5, 9, 13 and 17, respectively, the statistics of the matching results for the two sets of image pairs in Figure 7a,b are as shown in Figures 9 and 10, respectively. By analyzing the two resulting graphs, we can draw the following three conclusions. (1) Both image pairs achieve a relatively high matching accuracy at  $w = 3$  and  $w = 5$ , and reach the peak at  $m = 5$  under the condition of  $w = 5$ , while, for  $w = 3$ , both image pairs show a local peak at  $m = 5$ , respectively. (2) When  $w = 3$  and  $m > 5$ , although the matching accuracy of the image pair increases as  $m$  increases and it reaches the highest value in the parameter range at  $m = 17$ , the number of corresponding lines and the number of correct matches show a decreasing trend and also reach the lowest value at  $m = 17$ . (3) In addition, for  $m = 5$ , the number of corresponding lines and the number of correct matches are higher for  $w = 5$  compared to  $w = 3$ . In summary, it is easy to see that the matching results are better for two parameters with  $m = 5$  and  $w = 5$ .

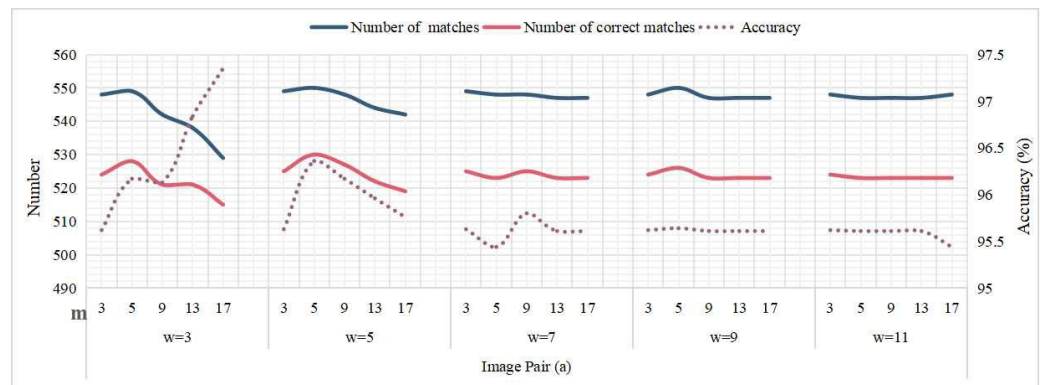


Figure 9. Performance of our approach with different  $m$  and  $w$  for Figure 7a image pair.

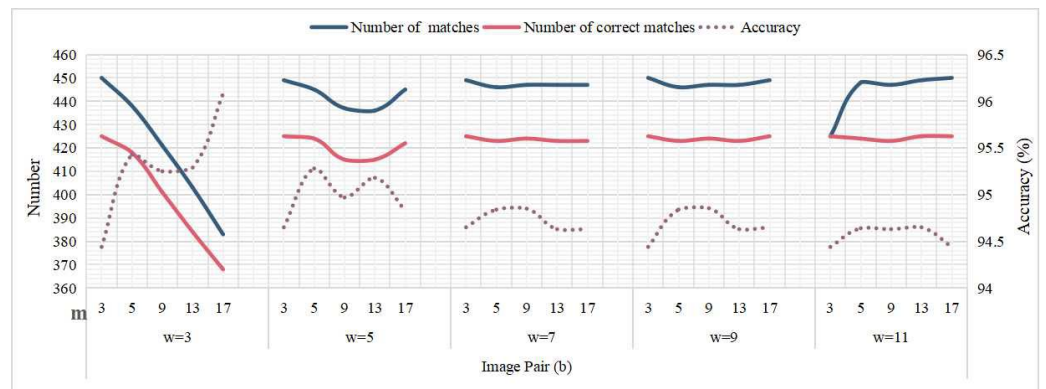


Figure 10. Performance of our approach with different  $m$  and  $w$  for Figure 7b image pair.

### 3.1.3. Determine the Values of Parameters $T_d$

$T_d$  is the threshold value of the Euclidean distance between the descriptors of the two lines, which is used to determine whether the two lines satisfy the similarity constraint. Given other parameter values, the two sets of images in Figure 7a,b are matched with the values of  $T_d$  at 0.3, 0.6, 0.9, 1.2 and 1.5, respectively, and the results are shown in Figure 11. In terms of the number of corresponding lines and the number of correct matches, both image pairs reach the maximum level of variation at  $T_d = 0.6$ , with a flat change after  $T_d = 0.6$ . The accuracy, on the other hand, gradually decreases with the increase in  $T_d$ , slowly leveling off and both varying within a small range, i.e., 95.62% to 98.22% and 94.43% to 95.65%. Thus, considering both the number of corresponding lines and the matching accuracy,  $T_d = 0.6$  is chosen in this paper.

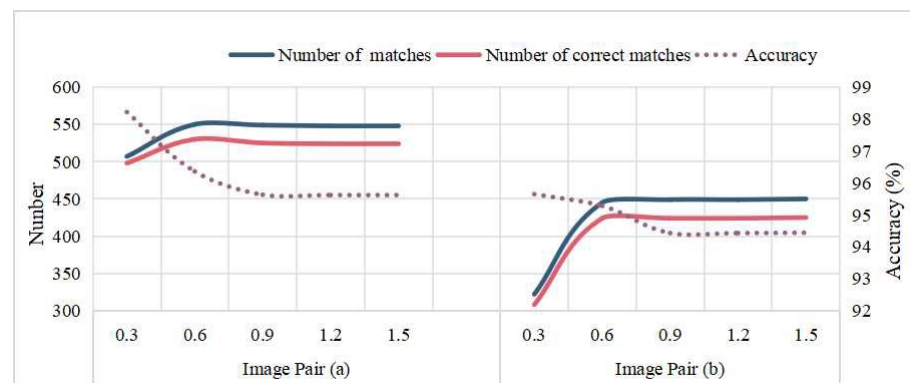


Figure 11. Performance of our approach with different  $T_d$  for Figure 7a,b image pairs.

### 3.2. Comparison to State-of-the-Art Matching Methods

To verify the effectiveness of the proposed approach, it was used to perform line matching experiments on the image pairs shown in Figure 7. We further compared our approach with state-of-the-art line matching approaches, the new line-point invariant (N-LPI) [13] and the Line-Junction-Line (LJL) [31] approaches. These two methods, which match line segments in groups and are mainly used for close-range images line matching, were employed for the comparison, because their source codes were available for download from the GitHub website. For each image pair, we used the same lines that were extracted by the LSD algorithm and corresponding points as input. Referring to reference [13,25], we evaluated the three approaches by computing the following three measures: the number of correct matches, the matching accuracy, and the running time, where accuracy is the ratio of the number of correct matches and total obtained matches. The statistics of the matching results of the three approaches are shown in Table 1. In the table, columns 1 to 4 represent, in order, the image pairs, the number of lines that are extracted from the reference

image, the number of lines that are extracted from the search image, and the number of corresponding points. The three numbers in column 5, respectively, indicate the number of corresponding lines, the number of correct matches and the matching accuracy in the result of our approach, and column 6 contains the running time of our approach. In addition, the corresponding experimental results from the LJL approach and the N-LPI approach are presented in columns seven to eight and nine to ten, respectively. To facilitate comparison and analysis, we further display the statistics in Figures 12 and 13. The line matching results using our approach for eight sets of image pairs are shown in Figure 14, where red lines indicate the incorrect matches and lines in other colors indicate the correct matches.

**Table 1.** Comparison of proposed approach and two state-of-the-art line matching approaches (LJL and N-LPI) for 8 image pairs.

Images	Line Number		Corresponding Point Number	Our Approach		LJL		N-LPI	
	Reference Images	Search Images		Number of Matches– Number of Correct Matches– Accuracy/%	Time/s	Number of Matches– Number of Correct Matches– Accuracy/%	Time/s	Number of Matches– Number of Correct Matches– Accuracy/%	Time/s
(a)	789	833	685	550–530–96.36	106	504–466–92.46	313	528–503–95.27	293
(b)	774	748	532	445–424–95.28	100	482–420–87.14	503	439–372–84.74	167
(c)	418	438	320	357–352–98.60	54	350–341–97.43	1395	355–351–98.87	121
(d)	782	764	374	489–449–91.82	105	486–412–84.77	1455	444–368–82.88	166
(e)	834	811	635	514–475–92.41	112	532–444–83.46	1019	491–437–89.00	260
(f)	578	610	295	352–329–93.47	69	330–313–94.85	215	350–344–98.29	260
(g)	718	699	442	370–358–96.76	87	360–337–93.61	670	344–323–93.90	146
(h)	428	553	607	292–287–98.29	52	316–283–89.56	83	301–274–91.03	67

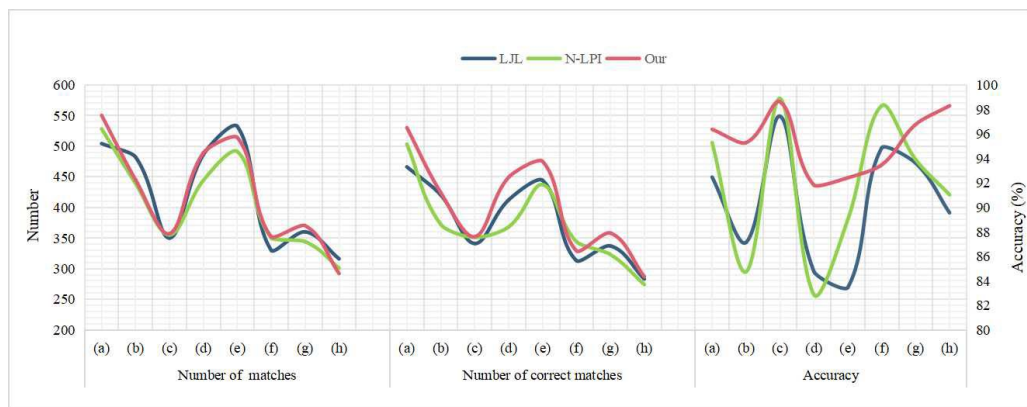


**Figure 12.** Number of matches, number of correct matches and accuracy obtained by three approaches for 8 image pairs. (a–h) are Figure 7a–h image pairs.

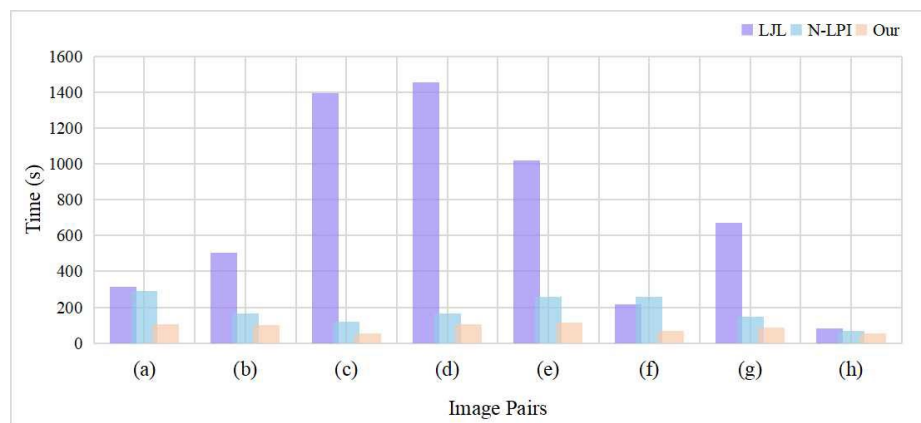


**Figure 13.** Running time of the three approaches for 8 image pairs. (a–h) are Figure 7a–h image pairs.

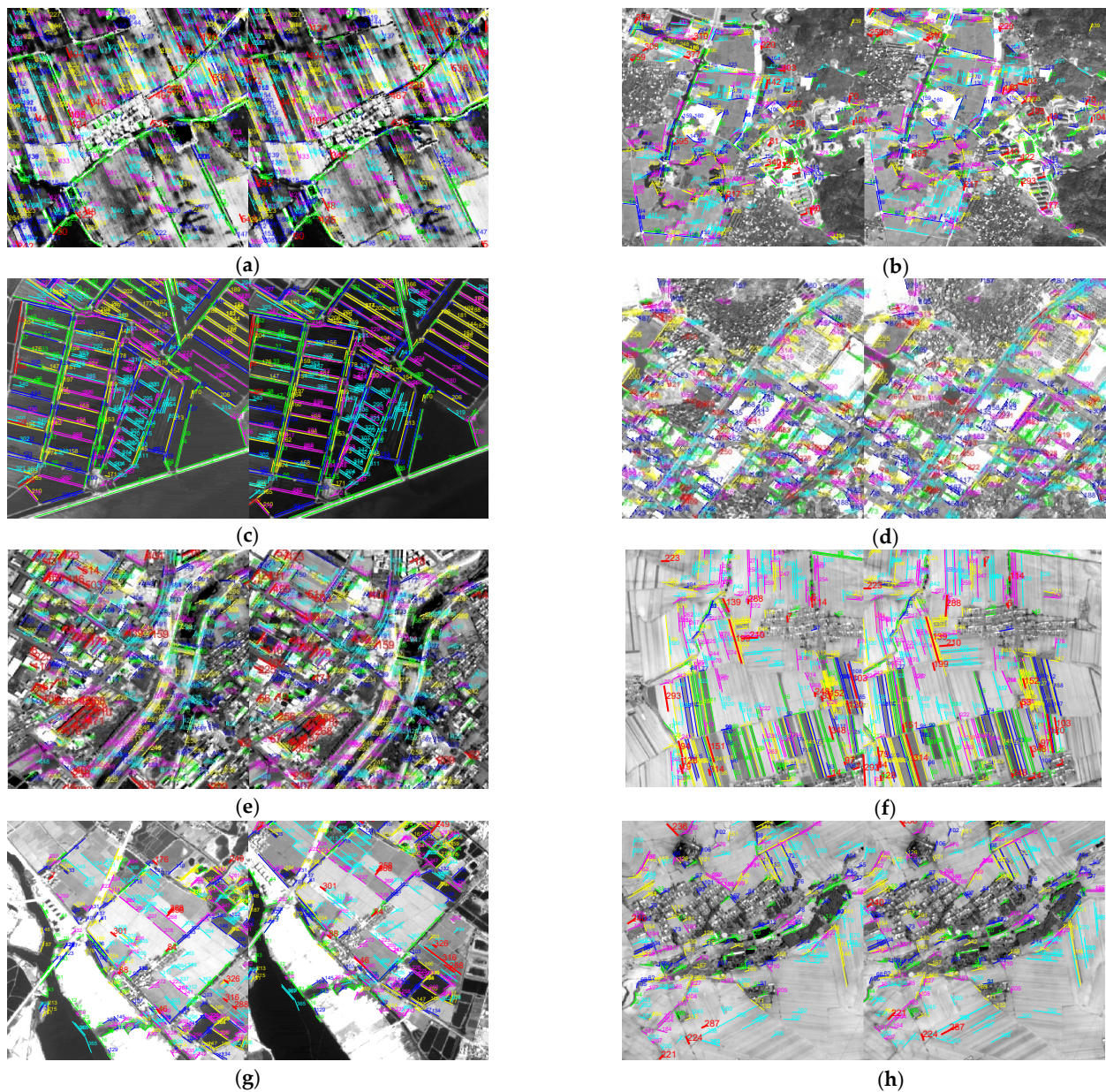


**Figure 14.** Results of line segment matching using our approach for 8 image pairs. The red lines indicate incorrect matches and lines in other colors indicate correct matches (a) Matches: 550; accuracy: 96.36% (b) Matches: 445; accuracy: 95.28% (c) Matches: 357; accuracy: 98.60% (d) Matches: 489; accuracy: 91.82% (e) Matches: 514; accuracy: 92.41% (f) Matches: 352; accuracy: 93.47% (g) Matches: 370; accuracy: 96.76% (h) Matches: 292; accuracy: 98.29%.

By comparing and analyzing the results, the following conclusions can be drawn. (1) In terms of the number of correct matches, the proposed approach has a higher number of correct matches than the other two approaches, except for image pair (f). In particular, for image pairs (a), (d) and (e), the number of correct matches of the proposed approach is 64, 37 and 31 more than the LJL approach, and 27, 81 and 38 more than the N-LPI approach, respectively. (2) In terms of accuracy, for eight sets of image pairs, the proposed approach's accuracy is above 91% and the average accuracy is higher than 95%. Except for image pairs (c) and (f), the accuracy of the proposed approach is higher than that of the other two approaches. For image pair (c), the accuracies of the three approaches are similar. For image pair (f), the accuracy of the proposed approach is 1.38% and 4.82% lower than that of the LJL and N-LPI approaches, respectively. (3) In terms of the running time, the proposed

approach has more obvious advantages over the other two approaches. For all eight image pairs, the average times of the LJI approach and the N-LPI approach are 8.25 times and 2.16 times longer than that of our approach, respectively. This is because the other two approaches require the extraction of line pairs that are assumed to be co-planar, which accounts for a large proportion of the overall matching time.

Combining the above statistics and the analysis of the matching results of the three approaches, it can be found that: (1) For a flat region with dense and well-distributed corresponding points, all three methods can obtain good matching results, such as image pairs (c). Despite the presence of a large number of neighboring parallel feature lines and light transformation on the image pair (c), the three approaches can still achieve a good matching result with over 97% accuracy. (2) The N-LPI approach yields false matches, mainly in areas with sparse or no corresponding points coverage. This is because this approach is based on corresponding points in the generation of matching primitives, the construction of geometric descriptors and the filtering of matching candidates with the homography matrix constraint, so the number and distribution of corresponding points have a strong influence on the approach. (3) The LJI approach can achieve better accuracy for flat areas or areas with less undulating terrain, such as image pairs (a), (c), (f) and (g), with an accuracy of over 90%, but for areas that are covered by buildings, which can easily result in false matches, such as image pairs (b), (d) and (e). This is because the approach assumes that the two lines in each pair are coplanar in object space and intersect in a local neighborhood, while in areas that have buildings with fractured textures on the image, non-coplanar lines that are misjudged as coplanar lead to an increase in false matches.

Compared with the other two approaches, our approach obtained lower accuracy in matching the image pair (f). Its false matches mainly occurred in regions with similar texture with only a few or no corresponding points. The corresponding points also play a key role in our approach, so it is difficult for our approach to obtain correct matches for regions of similar texture with few corresponding points. For the other seven sets of image pairs, our approach achieved more matches and higher accuracy, mainly due to the following advantages. (1) For the ZY-3 line array satellite image, in the matching process, our approach uses the RFM positive and inverse solution model to calculate the corresponding epipolar lines, which have high accuracy. (2) In our approach, during the construction of the line descriptor, on the one hand, the epipolar lines are used to determine the corresponding endpoints of the reference line and candidate line for constructing the corresponding line support regions. This solves the problem of inconsistent local support regions of corresponding lines due to extracted line breaks, thus improving the correspondence of the descriptors. On the other hand, the line descriptors are constructed separately on both sides of the line. This avoids the problem of no or false matches due to inconsistent information on both sides of the corresponding lines that is caused by large view changes, occlusion, etc. (3) Our approach uses the epipolar line constraint, direction constraint and corresponding points constraint in turn to narrow down the matching candidates to a small and reliable range. Furthermore, a double line descriptor similarity and point–line distance constraint are used to determine the final corresponding line. The multiple constraints in our approach effectively improve the number and correctness of the line matching results.

#### 4. Conclusions

This paper has presented a new line matching approach for high-resolution line array remote sensing images. The characteristics of our approach can be outlined as follows. (1) The epipolar line was fully exploited in our approach, mainly in the epipolar constraint and direction constraint to determine the matching candidates, and in the determination of the corresponding endpoints of the corresponding lines during the construction of the descriptors. (2) A double line descriptor is obtained by separately constructing a descriptor on each side of the line segment, which resolves the problem of inconsistency in the corresponding support regions of the corresponding lines on both images. (3) The corresponding

points are fully exploited in our approach, mainly in the point–line local geometric relationship constraint and the point–line distance similarity constraint, effectively avoiding the ambiguous matches that are generated by neighboring parallel lines. The proposed approach was tested for eight representative image patches that were selected from the ZY-3 line array satellite images, and the evaluation indicated that the proposed line matching approach could achieve promising results. For immediate future work, our aim is to achieve the rapid matching of large areas of line-array satellite remote sensing images.

**Author Contributions:** J.W. and P.Z. proposed the methodology and wrote the original manuscript; J.W. contributed to improving the methodology and is the corresponding author; S.L. contributed to the methodological testing and method improvement; J.W. and S.L. edited and improved the manuscript. All authors have read and agreed to the published version of the manuscript.

**Funding:** This work is supported by the National Natural Science Foundation of China with Project No. 41871379, and the LiaoNing Revitalization Talents Program with Project No. XLYC2007026.

**Acknowledgments:** We would like to thank the authors of Refs. [13,31] for providing the source code of their approaches. We are also very grateful for the valuable comments and contributions of the anonymous reviewers and members of the editorial team.

**Conflicts of Interest:** The authors declare no conflict of interest.

## References

- Lemaire, T.; Lacroix, S. Monocular-Vision Based SLAM Using Line Segments. In Proceedings of the 2007 IEEE International Conference on Robotics and Automation, Rome, Italy, 10–14 April 2007.
- Lyu, C.; Jiang, J. Remote sensing image registration with line segments and their intersections. *Remote Sens.* **2017**, *9*, 439. [[CrossRef](#)]
- Seok, B.R.; Hwang, Y.H.; Hong, H.K. 3D Reconstruction Based on Invariant Properties of 2D Lines in Projective Space. In *Advances in Intelligent Computing*; Springer: Berlin/Heidelberg, Germany, 2005.
- Qian, S.B.; Lin, Y. 3D reconstruction of rotated surface based on contour lines. *Comput. Eng. Des.* **2009**, *30*, 3875–3878. [[CrossRef](#)]
- Schindler, G.; Krishnamurthy, P.; Dellaert, F. Line-Based Structure from Motion for Urban Environments. In Proceedings of the Third International Symposium on 3D Data Processing, Visualization, and Transmission (3DPVT'06), Chapel Hill, NC, USA, 14–16 June 2006.
- Chen, M.; Shao, Z. Line-based matching for high-resolution images with robustness for scale, rotation and illumination. *Opt. Precis. Eng.* **2013**, *21*, 790–798. (In Chinese) [[CrossRef](#)]
- Elaksher, A.F. Automatic line matching across multiple views based on geometric and radiometric properties. *Appl. Geomat.* **2011**, *3*, 23–33. [[CrossRef](#)]
- Guerrero, J.J.; Sagüés, C. Robust Line Matching and Estimate of Homographies Simultaneously. In Proceedings of the Pattern Recognition and Image Analysis, First Iberian Conference, IbPRIA 2003, Puertode Andratx, Mallorca, Spain, 4–6 June 2003.
- Yip, R.K.K.; Ho, W.P. A multi-level dynamic programming method for stereo line matching. *Pattern Recognit. Lett.* **1998**, *19*, 839–855. [[CrossRef](#)]
- Zeng, J.X.; Yu, S.; Fu, X.; Li, C.X. A line segments matching method based on epipolar-line constraint and line segment features. *J. Softw.* **2011**, *6*, 1746–1754. [[CrossRef](#)]
- Song, W.D.; Zhu, H.; Wang, J.X.; Liu, Y.X. Line feature matching method based on multiple constraints for close-range images. *J. Image Graph.* **2016**, *21*, 764–770. (In Chinese)
- Wu, B.; Zhang, Y.; Zhu, Q. Integrated point and edge matching on poor textural images constrained by self-adaptive triangulations. *ISPRS J. Photogramm. Remote Sens.* **2012**, *68*, 40–55. [[CrossRef](#)]
- Jia, Q.; Fan, X.; Gao, X.K.; Yu, M.Y.; Li, H.J.; Luo, Z.X. Line matching based online-points invariant and local homography. *Pattern Recognit.* **2018**, *81*, 471–483. [[CrossRef](#)]
- Fan, B.; Wu, F.; Hu, Z. Robust line matching through line-point invariants. *Pattern Recognit.* **2012**, *45*, 794–805. [[CrossRef](#)]
- Zhang, Y.; Zhu, Q.; Wu, B.; Zou, Z. A hierarchical stereo line matching method based on a triangle constraint. *Geomat. Inf. Sci. Wuhan Univ.* **2013**, *38*, 522–527. (In Chinese)
- Fan, B.; Wu, F.; Hu, Z. Line Matching Leveraged by Point Correspondences. In Proceedings of the 23rd IEEE Conference on Computer Vision and Pattern Recognition, San Francisco, CA, USA, 13–18 June 2010.
- Ok, A.O.; Wegner, J.D.; Heipke, C.; Rottensteiner, F.; Soergel, U.; Toprak, V. A Stereo Line Matching Technique for Aerial Images Based on a Pair-Wise Relation Approach. In Proceedings of the ISPRS Istanbul Workshop 2010 on Modeling of Optical Airborne and Spaceborne Sensors, Istanbul, Turkey, 11–13 October 2010.
- Wang, Z.; Liu, H.; Wu, F. HLD: A robust descriptor for line matching. In Proceedings of the 2009 11th IEEE International Conference on Computer-Aided Design and Computer Graphics, Huangshan, China, 19–21 August 2009.
- Li, K.; Yao, J.; Lu, X. Robust Line Matching Based on Ray-Point-Ray Structure Descriptor. In Proceedings of the Asian Conference on Computer Vision, Singapore, 1–5 November 2014; Springer International Publishing: Cham, Switzerland, 2014.

20. Schmid, C.; Zisserman, A. Automatic Line Matching Across Views. In Proceedings of the IEEE Computer Society Conference on Computer Vision and Pattern Recognition, San Juan, PR, USA, 17–19 June 1997.
21. Bay, H.; Ferrari, V.; Gool, L.J.V. Wide-Baseline Stereo Matching with Line Segments. In Proceedings of the IEEE Computer Society Conference on Computer Vision and Pattern Recognition, San Diego, CA, USA, 20–26 June 2005.
22. Lowe, D.G. Distinctive image features from scale-invariant keypoints. *Int. J. Comput. Vis.* **2004**, *60*, 91–110. [[CrossRef](#)]
23. Wang, Z.; Wu, F.; Hu, Z. MSLD: A robust descriptor for line matching. *Pattern Recognit.* **2009**, *42*, 941–953. [[CrossRef](#)]
24. Verhagen, B.; Timofte, R.; Gool, L.V. Scale-Invariant Line Descriptors for Wide Baseline Matching. In Proceedings of the IEEE Winter Conference on Applications of Computer Vision, Steamboat Springs, CO, USA, 24–26 March 2014; pp. 493–500.
25. Zhang, L.; Koch, R. An efficient and robust line segment matching approach based on LBD descriptor and pairwise geometric consistency. *J. Vis. Commun. Image Represent.* **2013**, *24*, 794–805. [[CrossRef](#)]
26. Ok, A.O.; Wegner, J.D.; Heipke, C.; Rottensteiner, F.; Soergel, U.; Toprak, V. A new straight line reconstruction methodology from multi-spectral stereo aerial images. *Int. Arch. Photogramm. Remote Sens. Spat. Inf. Sci.* **2010**, *38*, 25–30.
27. Kim, H.; Lee, S. Simultaneous line matching and epipolar geometry estimation based on the intersection context of coplanar line pairs. *Pattern Recognit. Lett.* **2012**, *33*, 1349–1363. [[CrossRef](#)]
28. Wang, J.X.; Zhu, Q.; Wang, W.X. Reliable line matching algorithm for stereo images with topological relationship. *Acta Geod. Cartogr. Sin.* **2017**, *46*, 1850–1858. (In Chinese) [[CrossRef](#)]
29. Wang, J.X.; Zhu, Q.; Liu, S.Y.; Wang, W.X. Robust line feature matching based on pair-wise geometric constraints and matching redundancy. *ISPRS J. Photogramm. Remote Sens.* **2021**, *172*, 41–58. [[CrossRef](#)]
30. Wang, Q.; Chen, T.; Si, L. Sparse representation with geometric configuration constraint for line segment matching. *Neurocomputing* **2012**, *134*, 100–110. [[CrossRef](#)]
31. Li, K.; Yao, J.; Lu, X.H.; Li, L.; Zhang, Z.C. Hierarchical line matching based on Line–Junction–Line structure descriptor and local homography estimation. *Neurocomputing* **2016**, *184*, 207–220. [[CrossRef](#)]
32. Alshahri, M.; Yilmaz, A. Line matching in wide-baseline stereo: A top-down approach. *Image Processing IEEE Trans.* **2014**, *23*, 4199–4210. [[CrossRef](#)]
33. Wang, L.; Neumann, U.; You, S. Wide-Baseline Image Matching Using Line Signatures. In Proceedings of the IEEE International Conference on Computer Vision, Kyoto, Japan, 29 September–2 October 2009.
34. Park, S.H.; Lee, K.M.; Sang, U.K. A line feature matching technique based on an eigenvector approach. *Comput. Vis. Image Underst.* **2000**, *77*, 263–283. [[CrossRef](#)]
35. Ok, A.O.; Wegner, J.D.; Heipke, C.; Rottensteiner, F.; Soergel, U.; Toprak, V. Matching of straight line segments from aerial stereo images of urban areas. *ISPRS J. Photogramm. Remote Sens.* **2012**, *74*, 133–152. [[CrossRef](#)]
36. Gioi, R.G.V.; Jakubowicz, J.; Morel, J.M.; Randall, G. LSD: A fast line segment detector with a false detection control. *IEEE Trans. Pattern Anal. Mach. Intell.* **2010**, *32*, 722–732. [[CrossRef](#)] [[PubMed](#)]
37. Fischler, M.A.; Bolles, R.C. Random sample consensus: A paradigm for model fitting with applications to image analysis and automated cartography. *Commun. Assoc. Comp. Mach.* **1981**, *24*, 381–395. [[CrossRef](#)]
38. Dai, J.G.; Song, W.D.; Jia, Y.H.; Zhang, Q. A new automatically matching algorithm for multi-source high resolution optical satellite images. *Acta Geod. Cartogr. Sin.* **2013**, *52*, 2718–2726. (In Chinese) [[CrossRef](#)]